

Flexible neutral point displacement overvoltage suppression method based on backstepping control in unbalanced distribution networks

Ze-Yin Zheng^{1,2,*}, Jian-Feng Xu¹, Bin-Long Zhang¹, Hui Wang¹, Mou-Fa Guo^{1,2,**}, Shuyue Lin³

¹College of Electrical Engineering and Automation, Fuzhou University, Fuzhou 350108, China

²Engineering Research Center of Smart Distribution Grid Equipment, Fujian Province University, Fuzhou 350108, China

³Department of Engineering, University of Hull, Hull HU6 7RX, U.K.

*Corresponding authors: zhengzeyin@fzu.edu.cn

**Corresponding authors: gmf@fzu.edu.cn

Abstract: Three-phase AC distribution networks are required to operate as symmetrically as possible for optimal performance, but the three-phase-to-ground parameters are asymmetric in the field due to network construction deviation, resulting in the three-phase voltage unbalance and the neutral point displacement overvoltage. The neutral point displacement overvoltage would endanger the distribution networks and even damage critical power equipment. Therefore, the flexible asymmetry suppression device (FASD) with the topology of a cascaded H-bridge (CHB) inverter and the backstepping control (BSC) method is proposed for limiting the neutral point displacement overvoltage in this paper. The FASD outputs the current to the grid for compensating the unbalanced distribution networks caused by the asymmetry of three-phase-to-ground parameters and realizing the suppression of the neutral point displacement overvoltage. A current-based BSC method is designed to improve the stability and reliability of the CHB inverter, and the effectiveness of neutral point displacement overvoltage suppression based on the BSC method is verified by experimental results, and the advantage of the proposed method is shown by comparing with proportional-integral control (PIC) method, sliding mode control (SMC), and proportional resonant control (PRC) methods.

Keywords: Distribution networks; three-phase-to-ground parameters asymmetry; neutral point displacement overvoltage suppression; current injection; backstepping control.

1. INTRODUCTION

In modern power systems, three-phase AC is the most widely applied technology for high-power transmission [1, 2]. Theoretically, the three-phase voltages and currents have the same amplitude and the same frequency with a phase difference of 120 degrees. However, the three-phase unbalance is a common phenomenon in distribution networks [3]. Most of the consumer loads are single-phase, and these single-phase loads are unevenly distributed across the three phases. Since the single-phase loads are often connected to the nearest phases of the overhead line, it leads to voltage unbalance [4]. The 11kV overhead line designed two-phase method would increase the energy losses in distribution networks [5]. Even though the distribution networks are designed to be distributed symmetrically, the phase unbalance appears with loads being connected to the grid or disconnected from the grid [3, 6]. In addition, the random behavior of the load may lead to real-time voltage unbalance [3, 7]. The asymmetrical of mutual and self impedances which results in the structural asymmetries over three-phase is the intrinsic

feature of the imbalance of current and voltage in distribution networks [3, 8]. For the sake of obtaining representative residential low voltage feeders, the data set of 232 residential feeders in North West of England was selected as a case study [8]. The analysis for the data set indicates that the neutral current is determined by the type and number of customers. It was found that the phase imbalance in the Whitchurch area is larger during the period of the winter and at the daily demand peaks. Particularly, the asymmetry of the three-phase-to-ground parameters usually exists for a long time, which is one of the main reasons for the three-phase imbalance [9]. Furthermore, asymmetric faults are another factor contributing to the three-phase imbalance [3], but they are temporary phenomena and are usually resolved like dealing with faults [10, 11].

Unbalanced distribution networks often cause many problems. For example, owing to the phase with the least spare capacity depending on the usable capacity, the available capacity of feeders would be decreased by voltage imbalance. Similarly, the available capacity of transformers decreases because of the additional power consumption on the neutral lines [12]. In addition, there is an unbalanced voltage drops in the transformers and feeders [13]. These increase the additional reinforcement costs for the utility, which is not straightforward to get quantified [14]. Energy losses in lines and transformers are another consequence caused by the three-phase imbalance. The energy losses in the feeders are mainly composed of additional losses in the ground, and on the phases and neutral line. The energy losses of transformers are mainly occurred in their windings [3, 15]. To minimize power losses in unbalanced distribution networks, an optimal energy storage scheduling method satisfying the constraints of voltage and current was proposed in [16]. A statistical method was proposed to estimate the energy losses of distribution networks with scarce data, and these data were recorded annually [17]. The original data from [18] has been used to verify the Bayesian framework for estimating the energy losses caused by the phase imbalance [19]. A large number of distributed generators (DGs) are connected to the unbalanced distribution networks, which increases the additional energy losses. In [20], the impact of DGs on power loss and voltage profile was analyzed, and particle swarm optimization was applied to find the optimal allocation for power loss reduction.

Moreover, the stability of electrical devices is affected by unbalanced distribution networks. The output power of three-phase cascaded H-bridge (CHB) applied in high voltage and high power photovoltaic (PV) systems are different from each other in unbalanced distribution networks. It results in significant differences in heat dissipation requirements and service life of each module [21]. Furthermore, the additional heating and energy losses of generators arising from phase imbalance give rise to the generators overheating and even damage. The dynamic performance of generators differs greatly from that of phase balance [22]. An independent wind turbine-based double stator winding induction power generation system under the unbalanced load was introduced in [23]. It can adjust the positive sequence voltage of the load and remove the negative sequence voltage of the load at the same time. The positive voltage of the load is adjusted, meanwhile, the negative sequence current or active power double

frequency component of the load can be removed. Since the voltage imbalance has side effects on the normal operation of the static compensator, it leads to insufficient reactive power and the aggravation of unbalanced voltage [24].

The industry has been working on reducing the imbalance of distribution networks in recent years. The traditional method is to reconfigure the feeder using segment switches or to rebalance the phases through phase transposition [25]. However, the problem of unbalanced distribution networks cannot be completely solved due to the nonlinear effects of energy losses and voltage drops, so the simulated annealing was used to address the phase balance problem with the nonlinear effects [26]. In addition, a joint optimization model of static reactive power compensation equipment with Y-connection and delta-connection was proposed to minimize the active power loss in the unbalanced distribution networks, and the phase imbalance of whole networks rather than a single branch or a specific zone can be reduced [27]. Meanwhile, the current imbalance of transformers and the voltage imbalance of all three-phase nodes have been considered in the model, but it is only applicable to the three-phase four-wire pattern in low-voltage distribution networks. In [28], a three-phase electric spring was connected in series with noncritical loads to rebuild the new intelligent loads for mitigating the power imbalance and voltage fluctuation, but this method was not flexible enough and has poor applicability. Since DGs and loads with storage capacity are connected to the distribution networks, phase imbalance would be aggravated [23]. Therefore, distributed batteries included in rooftop PV systems are fully utilized to mitigate voltage imbalance [29]. However, these power electronic converters compensating voltage imbalance may cause the output active power oscillation and DC link voltage variations [30]. Moreover, the research on three-phase unbalance suppression mainly focuses on low-voltage distribution networks. As the upstream medium-voltage distribution networks, its imbalance is also necessary to be concerned. Despite that the imbalance caused by the asymmetry of three-phase-to-ground parameters is a long-standing issue, there are few studies about the suppression of imbalance. Therefore, it is significant to study the flexible asymmetry suppression method for limiting the neutral point displacement overvoltage.

To address the above problems, this paper proposes a method of neutral point displacement overvoltage suppression in unbalanced distribution networks based on an independent CHB inverter, which can withstand high voltage and output high-quality waveform. DC link voltage can be adjusted to adapt to different voltage levels in distribution networks. The research is based on the 10 kV distribution networks with the neutral point ungrounded or neutral point grounded by the Petersen coil, and the neutral point displacement overvoltage of these distribution networks is caused by asymmetry of three-phase-to-ground parameters. The CHB inverter with DC sources can inject current into distribution networks to suppress the neutral point displacement overvoltage for a long time, which can ensure the long-term phase balance operation of distribution networks. Considering that the backstepping control (BSC) has good stability and reliability for the CHB inverter [31], the current-based backstepping controller is designed to improve the performance of neutral point displacement overvoltage suppression.

This paper is organized as follows. The principle of the flexible neutral point displacement overvoltage suppression is introduced in Section 2. Section 3 presents the principle of current-based BSC for neutral point displacement overvoltage suppression. In Section 4, by numerical simulations, the performance of the neutral point displacement overvoltage suppression based on the BSC method is verified by comparison with based on proportional-integral control (PIC) method under different impact factors, including the damping coefficient, and resonance deviation of the Petersen coil, and three-phase-asymmetry coefficient of distribution networks. The experimental results are given in Section 5. Section 6 summarizes the conclusions.

2. PRINCIPLE OF FLEXIBLE NEUTRAL POINT DISPLACEMENT OVERVOLTAGE SUPPRESSION

A simplified equivalent distribution network with a neutral point grounded through a Petersen coil and flexible asymmetry suppression device (FASD) is demonstrated in Fig. 1. C_A , C_B , and C_C denote phase-to-ground capacitances. G_A , G_B , and G_C represent phase-to-ground conductances. Without loss of generality, the line impedances are ignored for simplified analysis. \dot{E}_A , \dot{E}_B , and \dot{E}_C are the phase electromotive forces. \dot{U}_A , \dot{U}_B , and \dot{U}_C are the phase-to-ground voltages. \dot{U}_0 is the neutral point voltage. L represent the inductance of the Petersen coil. The FASD includes n H-bridge cells. The DC-link of each H-bridge cell can be seen as the independent source. L_H is the filter inductance of the FASD. \dot{I}_H represents the output current of the FASD. K_H is the grid-connected breaker of the FASD.

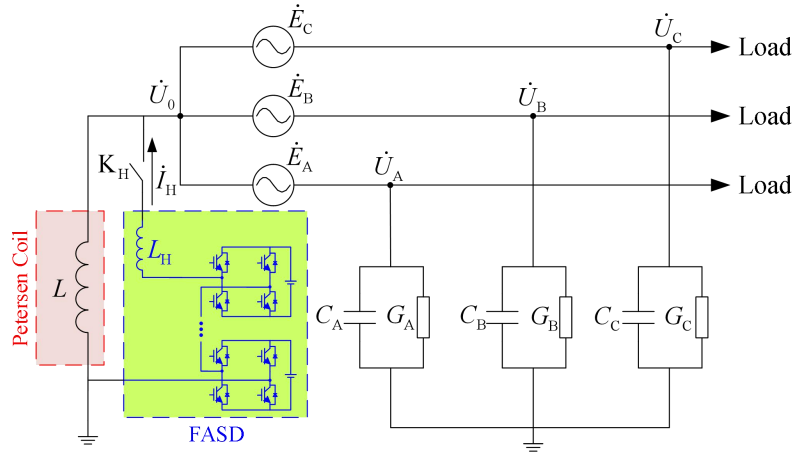


Fig. 1 Simplified equivalent distribution network with a neutral point grounded through the Petersen coil and the FASD.

With the breaker K_H open, the FASD is disconnected from the grid. According to Fig. 1 and Kirchoff's current law (KCL), it can be obtained that

$$\left(\dot{E}_A + \dot{U}_0\right)(j\omega C_A + G_A) + \left(\dot{E}_B + \dot{U}_0\right)(j\omega C_B + G_B) + \left(\dot{E}_C + \dot{U}_0\right)(j\omega C_C + G_C) + \frac{\dot{U}_0}{j\omega L} = 0. \quad (1)$$

where $\omega = 2\pi f$ and f is the grid frequency. Let

$$Y_X = j\omega C_X + G_X, Y_L = 1/(j\omega L), X = A, B, C \quad (2)$$

From (1) and (2), the neutral point displacement voltage \dot{U}_{00} is defined as

$$\dot{U}_{00} = -\frac{\dot{E}_A(Y_A + \alpha^2 Y_B + \alpha Y_C)}{Y_\Sigma + Y_L}. \quad (3)$$

where $\alpha = e^{j120}$, $Y_\Sigma = Y_A + Y_B + Y_C$. The unbalance degree of the distribution network is defined as $\beta = \dot{U}_{00}/\dot{E}_A$. From , if the phase-to-ground parameters of the distribution network are asymmetrical, it can be stated that $Y_A + \alpha^2 Y_B + \alpha Y_C \neq 0$ and $\dot{U}_{00} \neq 0$. If the phase-to-ground parameters of the distribution network are symmetrical, i.e., $Y_A = Y_B = Y_C = Y_0$, it can be obtained that $(\dot{E}_A + \dot{E}_B + \dot{E}_C)Y_0 = 0$ and $\dot{U}_{00} = 0$.

Typically, the asymmetry of phase-to-ground parameters is widespread in distribution networks. For the sake of suppressing the neutral point displacement overvoltage caused by the asymmetry of phase-to-ground parameters, the suppression current is injected into the grid by the grid-connected FASD with the K_H closing. In this case, should be rewritten as

$$(\dot{E}_A + \dot{U}_0)Y_A + (\dot{E}_B + \dot{U}_0)Y_B + (\dot{E}_C + \dot{U}_0)Y_C + \dot{U}_0 Y_L = \dot{I}_H. \quad (4)$$

When the reference value of injected current of the FASD is controlled as

$$\dot{I}_H = \dot{E}_A Y_A + \dot{E}_B Y_B + \dot{E}_C Y_C. \quad (5)$$

The neutral point voltage can be limited to zero. However, it is difficult to measure each phase-to-ground admittance directly. Combining and , it can be written into

$$\dot{I}_H = -\dot{U}_{00}(Y_\Sigma + Y_L). \quad (6)$$

From , the reference current of the FASD can be calculated without measuring each phase-to-ground parameter of the distribution network. Only the total phase-to-ground parameter of the distribution network is required to be measured. \dot{U}_{00} is the neutral point displacement voltage caused by the asymmetry of phase-to-ground parameters. \dot{U}_{00} can be measured before the FASD injects current into the grid. Similarly, in the case of the neutral point ungrounded of the distribution networks, the injected current can be obtained as

$$\dot{I}_H = -\dot{U}_{00} Y_\Sigma. \quad (7)$$

From and , in terms of the neutral point displacement overvoltage suppression based on the current method, it is essential to measure the total phase-to-ground parameter accurately. Thus, the precondition of implementing the function of suppressing the neutral point displacement overvoltage is required, that is, acquiring the total phase-to-ground parameter. The neutral point voltage is \dot{U}_0^{MP} after the FASD injects current \dot{I}_H^{MP} . According to Fig. 1 and KCL, the neutral point voltage can be expressed as

$$\dot{U}_0^{\text{MP}} = \frac{\dot{I}_H^{\text{MP}} - (\dot{E}_A Y_A + \dot{E}_B Y_B + \dot{E}_C Y_C)}{Y_\Sigma + Y_L}. \quad (8)$$

Combining and , it can be rewritten as

$$Y_\Sigma + Y_L = \frac{\dot{I}_H^{\text{MP}}}{\dot{U}_0^{\text{MP}} - \dot{U}_{00}}. \quad (9)$$

From , the total phase-to-ground parameter can be obtained by controlling the FASD to inject the current \dot{I}_H^{MP} . Similarly, in the case of the neutral point ungrounded of the distribution networks, it can be stated that

$$Y_\Sigma = \frac{\dot{I}_H^{\text{MP}}}{\dot{U}_0^{\text{MP}} - \dot{U}_{00}}. \quad (10)$$

It is notable that $\dot{U}_{00} = 0$ in and when three-phase-to-ground parameters are symmetrical.

3. BACKSTEPPING CONTROL METHOD DESIGN FOR FLEXIBLE NEUTRAL POINT DISPLACEMENT OVERVOLTAGE SUPPRESSION

The equivalent circuit diagram of the resonant grounded distribution network with the FASD is depicted in Fig. 2. u_H and i_H are the output voltage and the injected current of the FASD, respectively. u_L is the voltage drop across the filter inductor of the FASD. u_{rd} denotes the voltage disturbance, which is including the grid voltage disturbance. u_0 is the neutral point voltage. C_0 is the total phase-to-ground capacitance, which is the sum of C_A , C_B , and C_C . G_0 is the total phase-to-ground conductance, which is the sum of G_A , G_B , and G_C . L is the equivalent inductance of the Petersen coil. u_{00} is the neutral point displacement voltage.

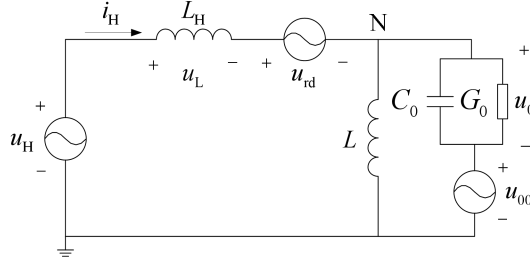


Fig. 2 Equivalent circuit diagram of resonant grounded distribution network with the FASD.

As illustrated in Fig. 2, according to KCL, it can be stated that

$$\frac{di_H}{dt} = \frac{u_H - u_0 - u_{rd}}{L_H}. \quad (11)$$

The output voltage of the FASD u_H can be expressed by the modulation coefficient K_{PWM} and modulation signal u_{con} , i.e., $u_H = K_{PWM}u_{con}$. Thus, (11) can be rewritten as

$$\frac{di_H}{dt} = -\frac{1}{L_H}u_0 + \frac{K_{PWM}}{L_H}u_{con} - \frac{1}{L_H}u_{rd}. \quad (12)$$

where u_{con} denotes the control signal of the FASD. Let $i_H = x(t)$, from (12), it can be obtained that

$$\begin{aligned} \frac{dx(t)}{dt} &= a_p u(t) + b_p g(t) + m(t) \\ &= (a_{pn} + \Delta a_{pn})u(t) + (b_{pn} + \Delta b_{pn})g(t) + m(t) \\ &= a_{pn}u(t) + b_{pn}g(t) + w(t) \end{aligned} \quad (13)$$

where $u(t) = u_0$, $g(t) = u_{con}$, $m(t) = -u_{rd}/L_H$, $a_{pn} = -1/L_H$, $b_{pn} = K_{PWM}/L_H$. a_{pn} and b_{pn} are the reference value of a_p and b_p , respectively. Δa_{pn} and Δb_{pn} are the deviation of a_p and b_p , respectively. $w(t) = \Delta a_{pn}u(t) + \Delta b_{pn}g(t) + m(t)$ is the total disturbance of the system.

According to (13), $g(t)$ can be stated that

$$g(t) = b_{pn}^{-1} \left(\frac{dx(t)}{dt} - a_{pn}u(t) - w(t) \right). \quad (14)$$

From (14), it can be constructed the function as

$$g(t) = b_{pn}^{-1} \left(\frac{dx_d(t)}{dt} - a_{pn}u(t) - c_g e_1 \right) + u_b. \quad (15)$$

In , $e_i = i_H - i_{H\text{ref}}$ denotes the current error, $x_d(t)$ is the reference value of the state variable, i.e., the reference current of the FASD. $u_b = -\rho b_{\text{pn}}^{-1} \text{sgn}(e_i)$ expresses the constructed function. ρ and c_g are the constant. $\text{sgn}(\cdot)$ is the sign function.

Substituting $u_b = -\rho b_{\text{pn}}^{-1} \text{sgn}(e_i)$ into , the equation can be described as

$$g(t) = \frac{L_H}{K_{\text{PWM}}} \left[\frac{di_{H\text{ref}}}{dt} + \frac{1}{L_H} u_0 - c_g (i_H - i_{H\text{ref}}) - \rho \text{sgn}(i_H - i_{H\text{ref}}) \right]. \quad (16)$$

When the output voltage of the FASD is controlled as $u_{\text{con}} = g(t)$, the injected current of the FASD can track the reference value $i_{H\text{ref}}$ steadily, and the control error will approach zero, i.e., $e_i = 0$. Then, the neutral point displacement overvoltage suppression can be achieved in the case of the neutral point ungrounded system or neutral resonant grounding system.

In order to design a suitable Lyapunov function, the stability of the BSC based on injected current method should be analyzed, which is shown as follows.

By substituting into , it can be described by

$$\frac{dx(t)}{dt} = \frac{dx_d(t)}{dt} - c_g e_i + b_{\text{pn}} u_b + w(t). \quad (17)$$

Then, the differential of the current control error can be expressed as

$$\frac{de_i(t)}{dt} = \frac{dx(t)}{dt} - \frac{dx_d(t)}{dt} = -c_g e_i + b_{\text{pn}} u_b + w(t). \quad (18)$$

The Lyapunov function can be designed as

$$V = \frac{1}{2} e_i^2. \quad (19)$$

The derivative of this Lyapunov function is

$$\frac{dV}{dt} = e_i \frac{de_i}{dt}. \quad (20)$$

Combining and , it can be stated that

$$\begin{aligned} \frac{dV}{dt} &= e_i \left[-c_g e_i + b_{\text{pn}} \left(-\rho b_{\text{pn}}^{-1} \text{sgn}(e_i) \right) + w(t) \right] \\ &= -c_g e_i^2 - \rho |e_i| + e_i w(t) \\ &\leq -c_g e_i^2 - \rho |e_i| + |e_i| |w(t)| \\ &= -c_g e_i^2 - |e_i| (\rho - |w(t)|). \end{aligned} \quad (21)$$

Where the sign function $\text{sgn}(\cdot)$ is the same sign as the independent variable. Therefore, $e_i \text{sgn}(e_i) = |e_i|$. When $c_g > 0$ and $|w(t)| \leq \rho$, $\rho > 0$, $dV/dt < 0$ and the system asymptotic stability is proved. Since the adjustment range of constant variables c_g and ρ are large, the designed BSC based on injected current method has strong adaptability.

As depicted in Fig. 3, the output current of the FASD is sampled as the feedback signal i_H . After the difference between the reference value i_{ref} and the feedback signal i_H is calculated, the modulated signal u_{con} can be obtained by the BSC method. After u_{con} is multiplied by the modulation coefficient K_{PWM} , the product is added to the neutral point voltage which is sampled by the potential transformer, and the sum is u_H . Finally, according to u_H , the FASD can be controlled by improved distributed commutation modulation (IDCM) strategy to the output voltage and realize the accurate tracking of the reference value i_{ref} .

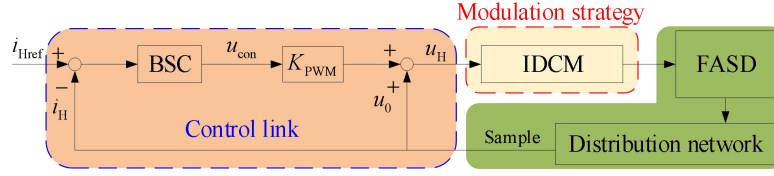


Fig. 3 Control diagram of the BSC based on the injected current method for suppressing the neutral point displacement overvoltage.

4. SIMULATION AND DISCUSSION

A simulation model of a 10 kV distribution network with a CHB inverter is shown in Fig. 4. OL denotes the overhead line with a length of 8 km, including OL1 to OL4. CL denotes the cable line with a length of 4 km, including CL1 to CL4. The parameters of overhead lines and cable lines are listed in Table I. C_A , C_B , and C_C denote the phase-to-ground capacitances. R_A , R_B , R_C denote the phase-to-ground leakage resistances. R_0 is the total phase-to-ground leakage resistance. d is the damping coefficient. β is the unbalance degree of the distribution network. In order to verify the adaptability of the proposed method with different topologies, it should consider the different damping coefficients and the unbalance degrees of the distribution network. Therefore, the feeders are set as different phase-to-ground parameters. K_{OL1} , K_{OL2} , K_{OL3} , and K_{OL4} mean the breakers of feeders whose line type is the overhead line. K_{CL1} , K_{CL2} , K_{CL3} , and K_{CL4} mean the breakers of feeders whose line type is cable line.

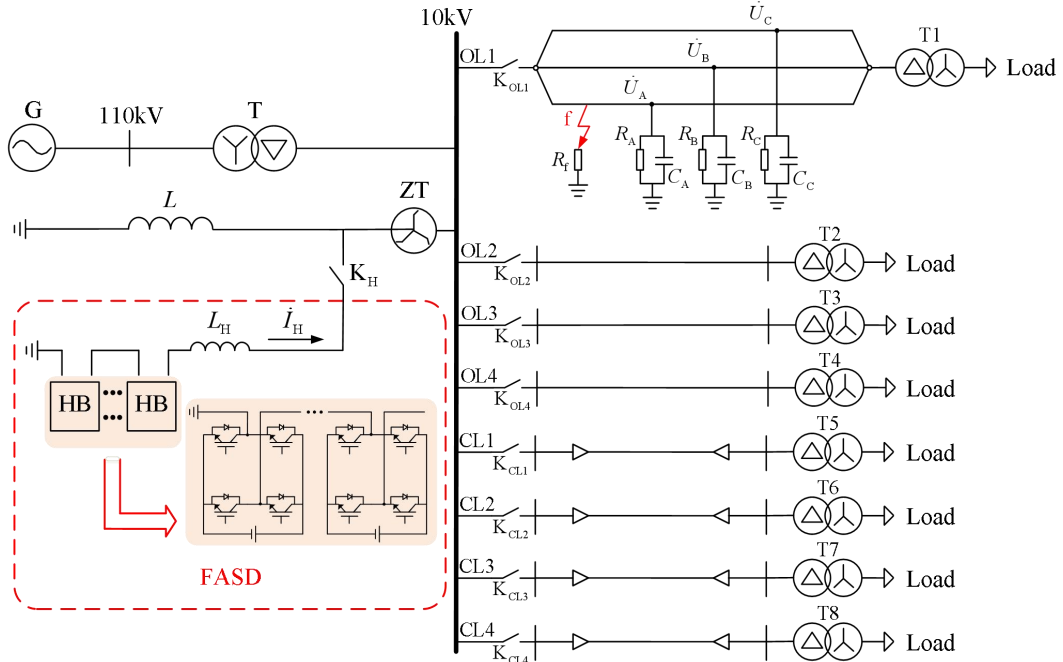


Fig. 4 Simulation model of 10 kV distribution network with the FASD.

Table I Line parameters

| Line Number | $C_A / \mu\text{F}$ | $C_B / \mu\text{F}$ | $C_C / \mu\text{F}$ | $R_0 / \text{k}\Omega$ | $d / \%$ | $\beta / \%$ |
|-------------|---------------------|---------------------|---------------------|------------------------|----------|--------------|
| OL1 | 0.074 | 0.079 | 0.084 | 450.00 | 2.98 | 4.13 |
| OL2 | 0.074 | 0.079 | 0.085 | 333.33 | 4.01 | 4.01 |
| OL3 | 0.074 | 0.079 | 0.091 | 440.00 | 2.96 | 4.98 |
| OL4 | 0.074 | 0.079 | 0.093 | 316.67 | 4.09 | 4.97 |
| CL1 | 1.220 | 1.320 | 1.370 | 20.33 | 4.00 | 4.00 |

| | | | | | | |
|-----|-------|-------|-------|-------|------|------|
| CL2 | 1.220 | 1.330 | 1.370 | 16.33 | 4.97 | 3.97 |
| CL3 | 1.220 | 1.350 | 1.410 | 20.00 | 4.00 | 5.02 |
| CL4 | 1.220 | 1.360 | 1.420 | 16.00 | 4.97 | 4.96 |

It is assumed that the breakers K_{OL1} and K_{CL1} in Fig. 4 are closed while others are opened. The waveforms of the neutral point displacement overvoltage suppression in different neutral point grounding modes are depicted in Fig. 5. u_0 is the neutral point voltage. i_H is the output current of the FASD. The proportional-integral controller is applied with the proportional coefficient $K_p = 350$ and the integral coefficient $K_i = 0.1$. In this case, when the asymmetrical line OL1 and CL1 are energized, the performance of the BSC method for suppressing the neutral point displacement overvoltage is shown in Fig. 6. The control parameters of the BSC method are set as $K_{PWM} = 60$, $c_g = 1$, and $\rho = 1$. The resonance deviation of the Petersen coil $\nu = \left(1 - 1/(\omega^2 LC_0)\right) \times 100$ is configured as 10%. The simulation time is 0.50 s.

As shown in Fig. 5 (a), before 0.10 s, due to the neutral point displacement overvoltage caused by the asymmetry of phase-to-ground parameters in the distribution network, the root mean square (RMS) of neutral point voltage reaches 1861 V. In particular, in the case of low resonance deviation of the Petersen coil, owing to the series resonance between the phase-to-ground capacitance and the Petersen coil, the neutral point displacement overvoltage is more distinguished. At $t = 0.10$ s, the FASD injects the compensation current to suppress the neutral point displacement overvoltage. During the initial stage of injected current, the output current of the FASD has a shock rise. It is because the output voltage of the FASD causes a sudden change in the neutral point voltage, but the current flowing through the Petersen coil cannot change instantly. Moreover, the low resonance deviation of the Petersen coil is prone to resonance, resulting in the output current rising. However, the amplitude of the inrush current is lower than 3 A, because the output time of the FASD is the zero-crossing of the reference current and the zero-crossing-current amplitude is low. The impulse current is gradually attenuated over two power frequency cycles. After 0.14s, the injected current i_H tends to be stable, and the zero-sequence voltage u_0 is suppressed stability. The RMS of u_0 is 53.13 V, and the suppression ratio of neutral point displacement voltage is 97.15%, where the suppression ratio is defined as the ratio of the reduced value of the neutral point voltage to the original value. Therefore, the impulse current has few impacts on suppressing neutral point displacement voltage.

As depicted in Fig. 5 (b), the RMS of neutral point displacement voltage is only 203.9 V before 0.10 s. This is attributed to the large phase-to-ground admittance in the case of the neutral point ungrounded. However, the neutral point displacement voltage caused by the asymmetry of phase-to-ground parameters cannot be ignored, which indicates great significance to investigate the methods for neutral point displacement overvoltage suppression. At $t = 0.10$ s, the FASD injects the compensation current, and there are no resonance and inrush currents due to the absence of the Petersen coil. Thus, the neutral point voltage is quickly limited to 1.95 V, and the suppression ratio reaches 99.04%.

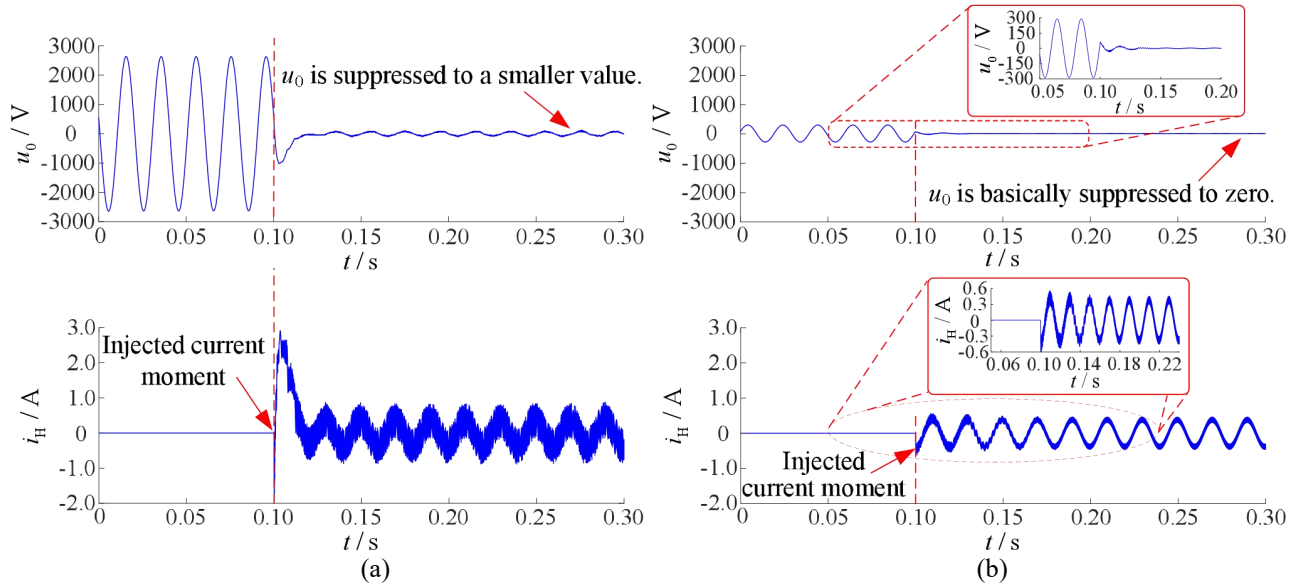


Fig. 5 Waveforms of suppressing the neutral point displacement overvoltage based on the PIC method under different neutral point grounding modes. (a) Neutral point grounded by the Petersen coil; (b) neutral point ungrounded.

Similarly, as illustrated in Fig. 6, before $t=0.1$ s, the neutral point displacement overvoltage is caused by the asymmetrical parameters of the distribution network. After $t=0.1$ s, the neutral point voltage is suppressed by injecting current. From Fig. 6 (a), the neutral point displacement overvoltage is large before 0.10 s. During the initial stage of injecting current by the FASD, an inrush output current is generated. From Fig. 6 (b), the neutral point displacement overvoltage is small before 0.10 s. Compared with the PIC method, the neutral point displacement overvoltage is not suppressed immediately by the BSC method but drops slowly. This is because the BSC method takes the modulation signal of the FASD as the control target, takes the reference current as the guide, and indirectly controls the output current. Furthermore, the BSC method considers the effect of the Petersen coil, so the process of neutral point displacement overvoltage suppression is relatively smooth, and the suppression performance is better than the PIC method.

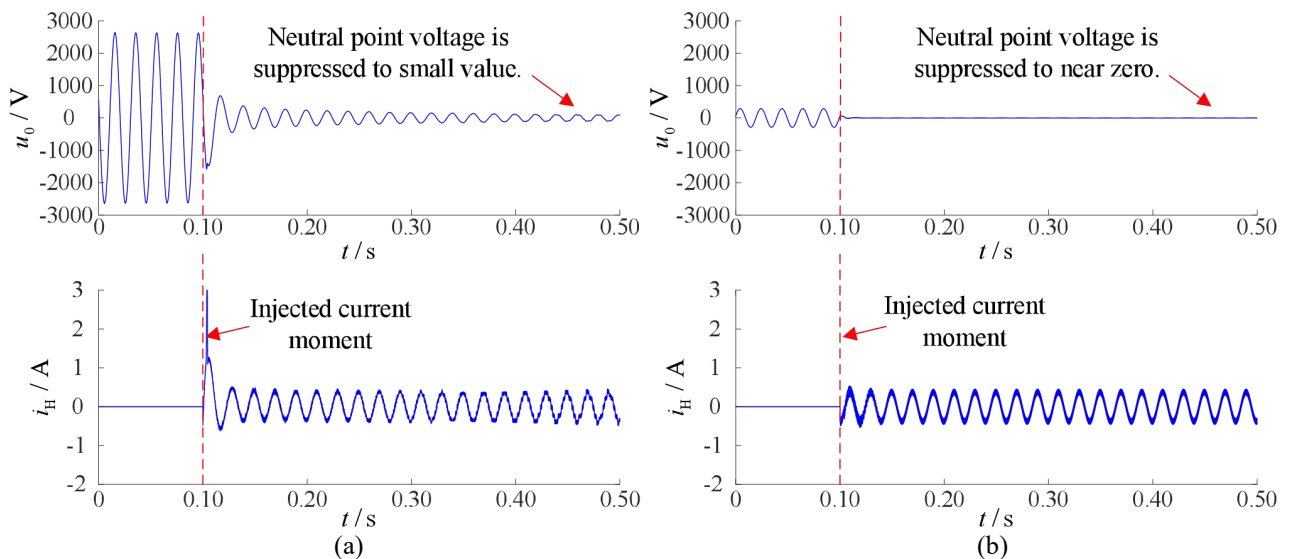


Fig. 6 Waveforms of suppressing the neutral point displacement overvoltage base on the BSC method. (a) Neutral point grounded by the Petersen coil; (b) neutral point ungrounded.

The effectiveness of suppressing the neutral point displacement overvoltage based on the PIC method in the case of neutral point grounded by the Petersen coil under different line combinations is listed in Table II. From Table II, the suppression ratio of neutral point displacement overvoltage can reach more than 97 % by the proposed method in the case of the neutral point grounded by the Petersen coil under different line combinations. In addition, the suppression ratio is slightly decreased as the damping coefficient increases, but the change of unbalance degree has no significant influence on the suppression of the neutral point displacement overvoltage.

Table II Comparison of the BSC and PIC methods in the case of the neutral point grounded by the Petersen coil under different line combinations.

| Overhead line | Cable line | $U_0^{\text{RMS-pre}}/\text{V}$ | $U_0^{\text{RMS-BSC}}/\text{V}$ | $U_0^{\text{RMS-PIC}}/\text{V}$ | $\eta^{\text{BSC}}/\%$ | $\eta^{\text{PIC}}/\%$ |
|---------------|------------|---------------------------------|---------------------------------|---------------------------------|------------------------|------------------------|
| OL1 | CL1 | 1861 | 46.51 | 53.13 | 97.50 | 97.15 |
| OL1 | CL2 | 1822 | 48.37 | 65.93 | 97.35 | 96.38 |
| OL1 | CL3 | 2293 | 64.52 | 64.56 | 97.19 | 97.18 |
| OL1 | CL4 | 2329 | 66.83 | 88.58 | 97.13 | 96.20 |
| OL2 | CL1 | 1867 | 47.10 | 55.05 | 97.48 | 97.05 |
| OL2 | CL2 | 1827 | 48.32 | 64.40 | 97.36 | 96.48 |
| OL2 | CL3 | 2297 | 64.92 | 75.27 | 97.17 | 96.72 |
| OL2 | CL4 | 2333 | 66.74 | 93.83 | 97.14 | 95.98 |
| OL3 | CL1 | 1929 | 51.94 | 57.74 | 97.31 | 97.01 |
| OL3 | CL2 | 1884 | 52.45 | 69.44 | 97.22 | 96.31 |
| OL3 | CL3 | 2357 | 65.45 | 76.17 | 97.22 | 96.77 |
| OL3 | CL4 | 2391 | 67.41 | 92.36 | 97.18 | 96.14 |
| OL4 | CL1 | 1945 | 52.31 | 54.24 | 97.31 | 97.21 |
| OL4 | CL2 | 1897 | 54.52 | 71.50 | 97.13 | 96.23 |
| OL4 | CL3 | 2371 | 66.48 | 76.24 | 97.20 | 96.78 |
| OL4 | CL4 | 2402 | 67.71 | 92.32 | 97.18 | 96.16 |

As shown in Table III, in the case of the neutral point ungrounded, the neutral point displacement voltages before and after suppression by the proposed method are listed under different line combinations. The suppression ratios are all more than 99 %. Similarly, the damping coefficient and unbalanced degree of the distribution network have little impact on the suppression ratio.

Table III Comparison of the BSC and PIC methods in the case of the neutral point ungrounded under different line combinations.

| Overhead line | Cable line | $U_0^{\text{RMS-pre}}/\text{V}$ | $U_0^{\text{RMS-BSC}}/\text{V}$ | $U_0^{\text{RMS-PIC}}/\text{V}$ | $\eta^{\text{BSC}}/\%$ | $\eta^{\text{PIC}}/\%$ |
|---------------|------------|---------------------------------|---------------------------------|---------------------------------|------------------------|------------------------|
| OL1 | CL1 | 203.9 | 1.290 | 1.950 | 99.37 | 99.04 |
| OL1 | CL2 | 206.3 | 1.303 | 1.989 | 99.37 | 99.04 |
| OL1 | CL3 | 251.6 | 1.421 | 2.343 | 99.44 | 99.07 |
| OL1 | CL4 | 263.8 | 1.484 | 2.433 | 99.44 | 99.08 |
| OL2 | CL1 | 204.9 | 1.298 | 1.992 | 99.37 | 99.03 |
| OL2 | CL2 | 207.3 | 1.305 | 1.978 | 99.37 | 99.05 |
| OL2 | CL3 | 252.6 | 1.447 | 2.369 | 99.43 | 99.06 |
| OL2 | CL4 | 264.8 | 1.463 | 2.471 | 99.45 | 99.07 |
| OL3 | CL1 | 211.3 | 1.316 | 1.995 | 99.38 | 99.06 |
| OL3 | CL2 | 213.3 | 1.308 | 2.035 | 99.39 | 99.05 |
| OL3 | CL3 | 258.7 | 1.463 | 2.392 | 99.43 | 99.08 |
| OL3 | CL4 | 270.7 | 1.511 | 2.472 | 99.44 | 99.09 |
| OL4 | CL1 | 213.4 | 1.304 | 2.042 | 99.39 | 99.04 |
| OL4 | CL2 | 215.3 | 1.327 | 2.054 | 99.38 | 99.05 |
| OL4 | CL3 | 260.7 | 1.477 | 2.418 | 99.43 | 99.07 |
| OL4 | CL4 | 272.7 | 1.517 | 2.531 | 99.44 | 99.07 |

The performances of neutral point displacement overvoltage suppression comparison of the PIC and BSC methods in the case of different resonance deviations of the Petersen coil are shown in Table IV. Before $t = 0.1$ s, the RMS of neutral point displacement voltage decreases with the increase of resonance deviation of the Petersen coil. This is attributed to the fact that the large resonance deviation of the Petersen coil indicates large equivalent admittance to the ground in distribution networks, and the neutral point displacement voltage becomes small after the equivalent admittance and the zero-sequence current act. After $t = 0.1$ s, the neutral point displacement voltage can be effectively suppressed in the case of different resonance deviations of the Petersen coil.

Table IV Comparison of the BSC and PIC methods under different resonance deviations of the Petersen coil.

| L/H | $\nu/\%$ | $U_0^{\text{RMS-pre}}/\text{V}$ | $U_0^{\text{RMS-PIC}}/\text{V}$ | $U_0^{\text{RMS-BSC}}/\text{V}$ | $\eta^{\text{PIC}}/\%$ | $\eta^{\text{BSC}}/\%$ |
|-------|----------|---------------------------------|---------------------------------|---------------------------------|------------------------|------------------------|
| 2.386 | 2 | 4418 | 133.20 | 47.16 | 96.99 | 98.93 |
| 2.317 | 5 | 3102 | 93.74 | 47.41 | 96.98 | 98.47 |
| 2.253 | 8 | 2235 | 61.84 | 46.19 | 97.23 | 97.93 |
| 2.212 | 10 | 1861 | 53.13 | 46.51 | 97.15 | 97.50 |

5. EXPERIMENTAL RESULTS

The proposed method was validated using a laboratory prototype including a physical simulation system of the distribution network, an adjustable transformer, and a prototype of the FASD which is the topology of a 25-level CHB inverter. The schematic diagram and photograph of the experimental platform hardware are demonstrated in Fig. 7. The experimental parameters and line parameters are listed in Table V and Table VI, respectively. The total phase-to-ground leakage resistance is denoted as R_0 . The three-phase-asymmetry coefficient is expressed as $K_C = \left| \frac{C_A + \alpha^2 C_B + \alpha C_C}{C_A + C_B + C_C} \right| \times 100$. The damping coefficient is defined as $d = 1/(\omega R_0 C_0)$.

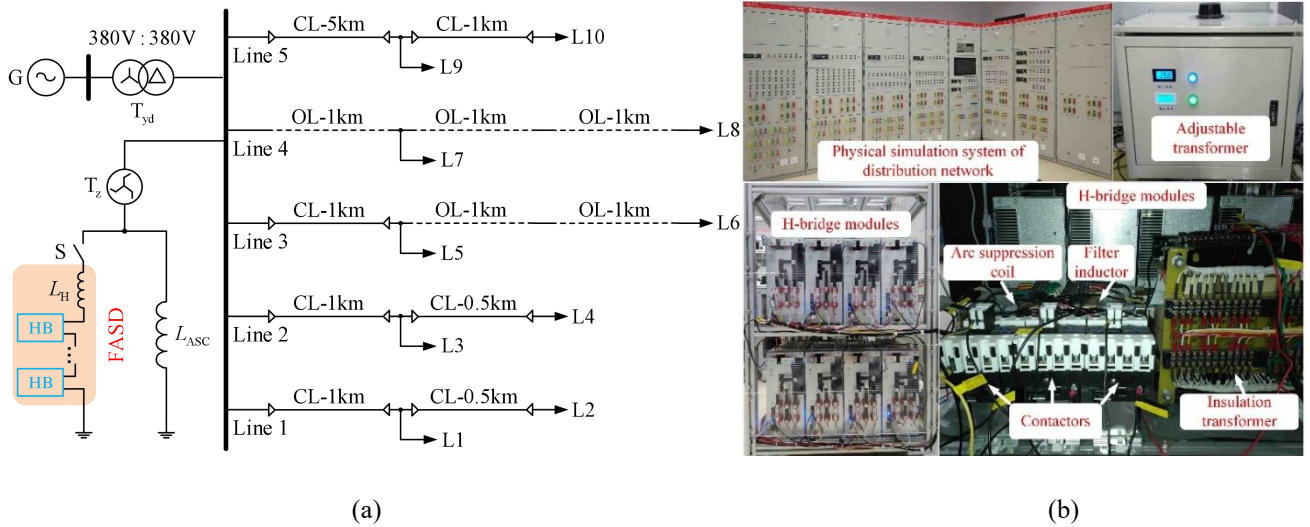


Fig. 7 Experimental test-rig for the prototype of the FASD.

Table V Line parameters in the experiment.

| Line number | $C_A / \mu\text{F}$ | $C_B / \mu\text{F}$ | $C_C / \mu\text{F}$ | $R_0 / \text{k}\Omega$ | $d / \%$ | $K_C / \%$ |
|-------------|---------------------|---------------------|---------------------|------------------------|----------|------------|
|-------------|---------------------|---------------------|---------------------|------------------------|----------|------------|

| | | | | | | |
|--------|-------|-------|-------|------|------|-------|
| Line 1 | 11.15 | 15.85 | 11.15 | 3.33 | 2.50 | 12.32 |
| Line 2 | 6.45 | 15.85 | 6.45 | 3.33 | 3.32 | 32.70 |
| Line 3 | 4.70 | 14.10 | 4.70 | 3.33 | 3.97 | 40.00 |
| Line 4 | 6.45 | 11.15 | 6.45 | 3.33 | 4.06 | 19.54 |
| Line 5 | 4.70 | 9.40 | 4.70 | 3.33 | 5.08 | 25.00 |

Table VI Experimental parameters.

| Description | Value |
|--|-------------|
| Line-to-line voltage | 0.4 [kV] |
| Filter inductance L_H | 58.33 [mH] |
| A DC-link voltage of each HB V_{dc} | 50 [V] |
| Switching frequency f_s | 6 [kHz] |
| Sampling frequency | 18 [kHz] |
| Inductance of arc suppression coil L | 202.69 [mH] |
| Cascaded numbers N | 12 |

Three different scenarios are performed for comparing different control methods. The parameters of these scenarios are listed in Table VII. In order to compare the performance of different control methods on suppressing the neutral point displacement overvoltage, different damping coefficients, different three-phase-asymmetry coefficients, and different resonance deviations of the Petersen coil are considered in the three scenarios. Note that in the case of Scenario 3, the waveforms suppressing the neutral point displacement overvoltage based on the PIC method, and sliding mode control (SMC) method [32], which is based on exponential approach law, and proportional resonant control (PRC) method [33], and BSC method are depicted in Fig. 8, and Fig. 9, and Fig. 10, and Fig. 11, respectively. The CHB output voltage, neutral point voltage, and CHB output current responses for comparing different control methods for suppressing the neutral point displacement overvoltage are shown in Fig. 8(a)-Fig. 11(a) under the case of the neutral point grounded by the Petersen coil. Under the case of the neutral point ungrounded, they are illustrated in Fig. 8(b)-Fig. 11(b). Furthermore, the results of the three scenarios are given in Table VIII and Table IX.

The output voltage of the FASD is denoted as u_H . The neutral point voltage is denoted as u_0 . The output current of the FASD is denoted as i_H . The control parameters of the PIC method are configured as $K_p = 50$ and $K_I = 0.01$. The control parameters of the SMC method are set as $\eta_{SMC} = 3000$ and $\varepsilon_{SMC} = 1$. The control parameters of the PRC method are configured as $K_p = 70$, and $K_R = 1$, and $\omega_0 = 100\pi$. The control parameters of the BSC method are set as $K_{PWM} = 1$, and $c_g = 2000$, and $\rho = 1$.

Table VII Parameters in different scenarios.

| Scenario number | $C_A / \mu\text{F}$ | $C_B / \mu\text{F}$ | $C_C / \mu\text{F}$ | $R_0 / \text{k}\Omega$ | $d / \%$ | $K_C / \%$ |
|-----------------|---------------------|---------------------|---------------------|------------------------|----------|------------|
| Scenario 1 | 6.4467 | 11.1967 | 6.4467 | 3.33 | 3.96 | 19.72 |
| Scenario 2 | 6.4467 | 15.9467 | 6.4467 | 3.33 | 3.31 | 32.94 |
| Scenario 3 | 6.4467 | 20.6967 | 6.4467 | 3.33 | 2.84 | 42.42 |

As demonstrated in Fig. 8 (a), the RMS of the neutral point voltage caused by the asymmetry of phase-to-ground parameters is 91.30 V before the FASD injects current. After injecting the current, the neutral point voltage is limited to 15.98 V and the suppression ratio is 82.50 %. From Fig. 8 (b), the RMS of the neutral point voltage is 189.50 V before injecting the current. The neutral point voltage is suppressed to 35.00 V and the suppression ratio is 81.53 % after injecting the current. From

Fig. 8, it can be obtained that before the FASD injects current, the neutral point voltage in the case of the neutral point grounded by the Petersen coil is slightly higher than that in the case of the neutral point ungrounded.

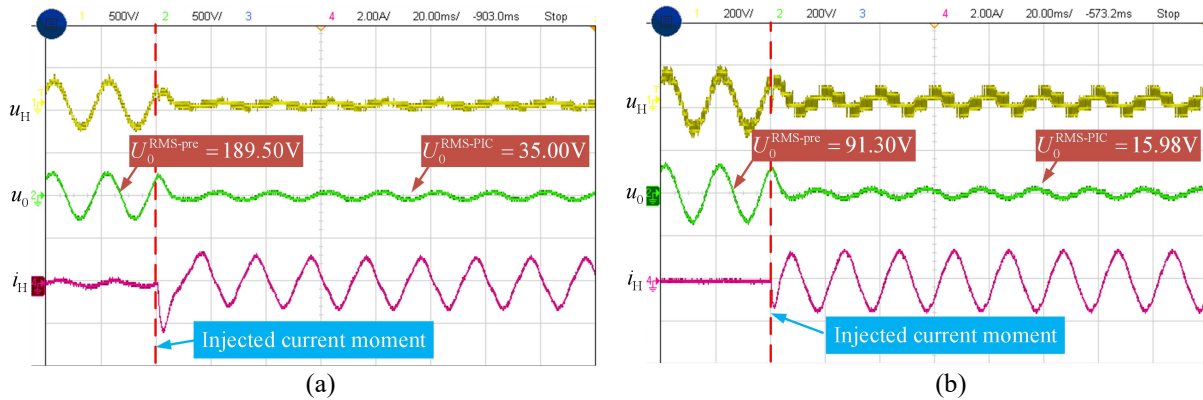


Fig. 8 Waveforms of the neutral point displacement overvoltage suppression based on the PIC method (experimental results). (a) Neutral point grounded by the Petersen coil; (b) neutral point ungrounded.

As demonstrated in Fig. 9 (a), the RMS of the neutral point voltage caused by the asymmetry of phase-to-ground parameters is 190.50 V before the FASD injects current. After injecting the current, the neutral point voltage is limited to 39.70 V and the suppression ratio is 79.16 %. From Fig. 9 (b), the RMS of the neutral point voltage is 91.79 V before injecting the current. The neutral point voltage is suppressed to 15.49 V and the suppression ratio is 83.12 % after injecting the current.

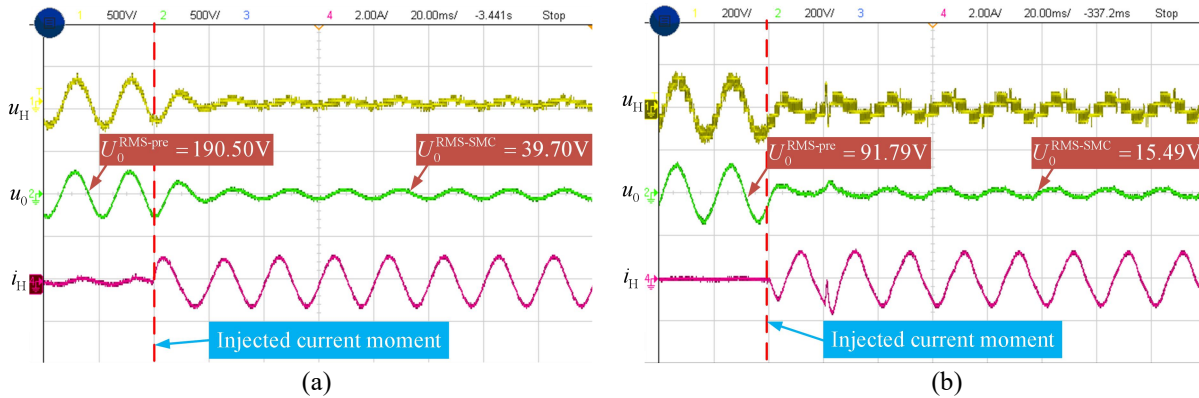


Fig. 9 Waveforms of the neutral point displacement overvoltage suppression based on the SMC method (experimental results). (a) Neutral point grounded by the Petersen coil; (b) neutral point ungrounded.

As demonstrated in Fig. 10(a), the RMS of the neutral point voltage caused by the asymmetry of phase-to-ground parameters is 188.30 V before the FASD injects current. After injecting the current, the neutral point voltage is limited to 37.50 V and the suppression ratio is 80.08 %. From Fig. 10(b), the RMS of the neutral point voltage is 91.25 V before injecting the current. The neutral point voltage is suppressed to 15.51 V and the suppression ratio is 83.00 % after injecting the current.

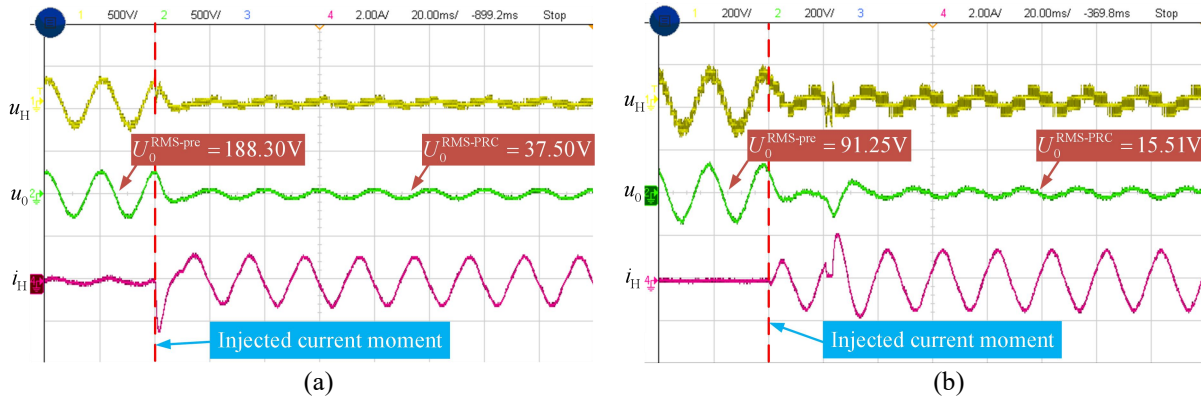


Fig. 10 Waveforms of the neutral point displacement overvoltage suppression based on the PRC method (experimental results). (a) Neutral point grounded by the Petersen coil; (b) neutral point ungrounded.

By observing Fig. 11, either in the case of the neutral point grounded via the Petersen coil or the case of the neutral point ungrounded, the neutral point displacement overvoltage can be suppressed effectively once the FASD injects the appropriate current into the grid. As illustrated in Fig. 11 (a), after the FASD injects current, the suppression ratio is up to 83.08 % in the case of the neutral point grounded via the Petersen coil. The neutral point voltage tends to be stable after one power frequency cycle. However, the suppression ratio is as much as 83.33 % in the case of the neutral point ungrounded as displayed in Fig. 11 (b). It only has one power frequency cycle of oscillation for the neutral point voltage to stabilize. Comparing with Fig. 8, Fig. 9, Fig. 10, and Fig. 11, although the stabilization time based on the BSC method is longer than that based on the PIC method, the suppression ratio based on the BSC method is better than that based on PIC, SMC, and PRC method. Furthermore, experimental results indicate that the effectiveness of suppressing the neutral point displacement overvoltage based on the BSC method in the case of the neutral point ungrounded is better than that in the case of the neutral point grounded by the Petersen coil.

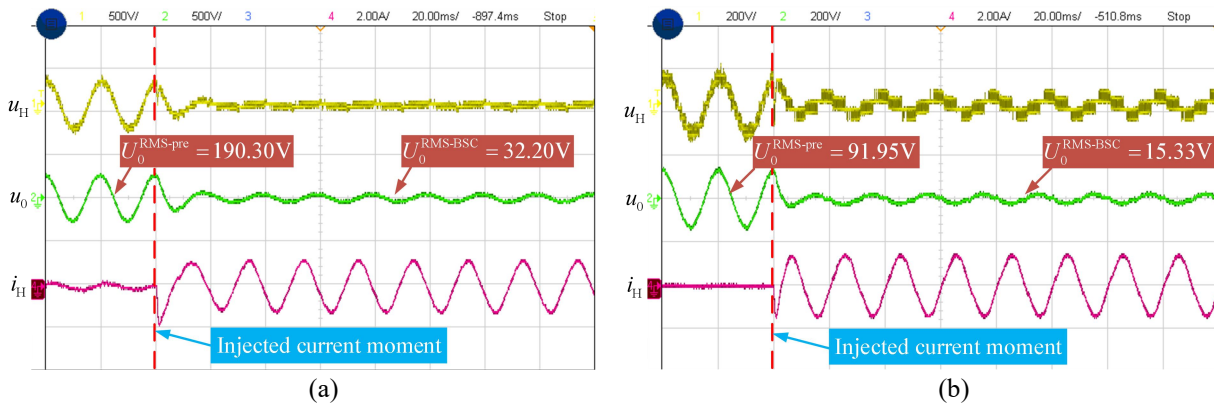


Fig. 11 Waveforms of the neutral point displacement overvoltage suppression based on the BSC method (experimental results). (a) Neutral point grounded by the Petersen coil; (b) neutral point ungrounded.

As shown in Table VIII and Table IX, in the case of the neutral point ungrounded, the suppression ratios based on the BSC method are higher than 67 %. In the case of the neutral point grounded via the Petersen coil, the suppression ratios are increased with the rise of the damping coefficients. In comparison with the PIC, SMC, and PRC methods, the suppression ratios based on the BSC method have no significant increase. However, in the case of the neutral point ungrounded, the BSC method to

suppress the neutral point displacement overvoltage can achieve a higher suppression ratio and lower the neutral point voltage in comparison with the PIC, SMC, and PRC methods.

Table VIII Comparison of the PIC, SMC, PRC, and BSC methods for suppressing the neutral point displacement overvoltage in the case of the neutral point grounded by the Petersen coil (experimental results).

| Control method | Scenario 1 | | | Scenario 2 | | | Scenario 3 | | |
|----------------|--------------------------|---------------------------|-----------|--------------------------|---------------------------|-----------|--------------------------|---------------------------|-----------|
| | $U_0^{\text{RMS-pre}}/V$ | $U_0^{\text{RMS-post}}/V$ | $\eta/\%$ | $U_0^{\text{RMS-pre}}/V$ | $U_0^{\text{RMS-post}}/V$ | $\eta/\%$ | $U_0^{\text{RMS-pre}}/V$ | $U_0^{\text{RMS-post}}/V$ | $\eta/\%$ |
| PIC | 39.16 | 13.33 | 65.96 | 100.72 | 22.41 | 77.75 | 189.50 | 35.00 | 81.53 |
| SMC | 39.13 | 13.16 | 66.37 | 100.69 | 23.57 | 76.59 | 190.50 | 39.70 | 79.16 |
| PRC | 38.71 | 12.89 | 66.70 | 100.86 | 24.14 | 76.07 | 188.30 | 37.50 | 80.08 |
| BSC | 38.84 | 12.12 | 68.80 | 100.80 | 19.68 | 80.48 | 190.30 | 32.20 | 83.08 |

Table IX Comparison of the PIC, SMC, PRC, and BSC methods for suppressing the neutral point displacement overvoltage in the case of the neutral point ungrounded (experimental results).

| Control method | Scenario 1 | | | Scenario 2 | | | Scenario 3 | | |
|----------------|--------------------------|---------------------------|-----------|--------------------------|---------------------------|-----------|--------------------------|---------------------------|-----------|
| | $U_0^{\text{RMS-pre}}/V$ | $U_0^{\text{RMS-post}}/V$ | $\eta/\%$ | $U_0^{\text{RMS-pre}}/V$ | $U_0^{\text{RMS-post}}/V$ | $\eta/\%$ | $U_0^{\text{RMS-pre}}/V$ | $U_0^{\text{RMS-post}}/V$ | $\eta/\%$ |
| PIC | 41.20 | 14.27 | 65.36 | 70.19 | 14.17 | 79.81 | 91.30 | 15.98 | 82.50 |
| SMC | 41.02 | 13.87 | 66.19 | 70.40 | 14.04 | 80.06 | 91.79 | 15.49 | 83.12 |
| PRC | 41.04 | 13.64 | 66.76 | 70.34 | 13.89 | 80.25 | 91.25 | 15.51 | 83.00 |
| BSC | 41.14 | 13.23 | 67.84 | 70.25 | 13.66 | 80.56 | 91.95 | 15.33 | 83.33 |

6. CONCLUSIONS

This paper presents a neutral point displacement overvoltage suppression method based on the independent CHB inverter to correct unbalanced distribution networks. The corresponding current-based backstepping controller is designed to improve the performance of neutral point displacement overvoltage suppression. The current-based BSC method has better performance for suppressing the neutral point displacement overvoltage than proportional-integral control (PIC), sliding mode control (SMC), and proportional-resonant control (PRC) methods, under different impact factors, including the damping coefficient, resonance deviation of the Petersen coil, and three-phase-asymmetry coefficient of distribution networks.

It is worth mentioning that the proposed method would impact the protection of single-phase-to-ground (SPG) fault during the process of suppressing the neutral point displacement overvoltage. When the SPG fault occurs during the process of suppressing the neutral point displacement overvoltage, the variation of zero-sequence voltage caused by the SPG fault would be attenuated by the proposed method, especially, in the case of high resistance grounding fault. It has side effects on the accuracy of the diagnosis of SPG fault in the protection device. Therefore, it is necessary to research the influences and requirements of the triggering method of SPG fault in the protection device, which will be the research work in the future.

7. ACKNOWLEDGMENTS

This work is supported in part by the National Natural Science Foundation of China under Award 51677030. Furthermore, the authors express their sincere gratitude to the Referees and the Associate Editor for their thoroughness in reviewing this manuscript and their valuable advice.

8. REFERENCES

- [1] Lin B R, Yang T Y. Analysis and implementation of three-phase power quality compensator under the balanced and unbalanced load conditions[J]. *Electr Power Syst Res* 2006, 76(5): 271-282.
- [2] Zhang L, Yang H X, Tang Y, Pou J, Tolbert L M. Decoupled Modulation With Common-Mode Load-Voltage Control for Three-Phase Four-Leg Three-Level Inverter[J]. *IEEE Trans Ind Electron* 2021, 69(8): 8594-8598.
- [3] Siti M W, Nicolae D V, Jimoh A A, Ukil A. Reconfiguration and load balancing in the LV and MV distribution networks for optimal performance[J]. *IEEE Trans Power Del* 2007, 22(4): 2534-2540.
- [4] SP Energy Networks. (2015, Sep.). HV and LV Phase Imbalance Assessment [Online]. Available: <https://www.spenergynetworks.co.uk/userfiles/file/HVandLVPhaseImbalanceAssessment16.pdf>
- [5] G. Strbac et al., "Management of electricity distribution network losses," 2014. [Online]. Available: <https://www.westernpower.co.uk/downloads/4847>
- [6] Rodrigues H M, Melo I D, Nepomuceno E G. An interval power flow for unbalanced distribution systems based on the Three-Phase Current Injection Method[J]. *Int J Electr Power Energy Syst* 2022, 139: 107921.
- [7] Mokryani G, Majumdar A, Pal B C. Probabilistic method for the operation of three-phase unbalanced active distribution networks[J]. *IET Renewable Power Gener* 2016, 10(7): 944-954.
- [8] Righi V, Ochoa L F, Chicco G, Navarro-Espinosa A. Representative residential LV feeders: A case study for the North West of England[J]. *IEEE Trans Power Syst* 2015, 31(1): 348-360.
- [9] Gargoom A, Oo A M T, Cavanagh M. A method for calculating the asymmetry in the shunt parameters of power lines in compensated distribution networks[J]. *IEEE Trans Power Del* 2019, 35(5): 2168-2176.
- [10] Kalyuzhny A. Analysis of temporary overvoltages during open-phase faults in distribution networks with resonant grounding[J]. *IEEE Trans Power Del* 2014, 30(1): 420-427.
- [11] Bracale A, Caramia P, De Falco P, Di Fazio A R. Short-circuit modeling of three-phase 4-wire unbalanced networks in presence of single-phase photovoltaic systems[J]. *Int J Electr Power Energy Syst* 2022, 135: 107604.
- [12] Ma K, Li R, Li F R. Quantification of additional asset reinforcement cost from 3-phase imbalance[J]. *IEEE Trans Power Syst* 2015, 31(4): 2885-2891.
- [13] Ma K, Li F R, Aggarwal R. Quantification of additional reinforcement cost driven by voltage constraint under three-phase imbalance[J]. *IEEE Trans Power Syst* 2016, 31(6): 5126-5134.
- [14] Ma K, Li R, Li F R. Utility-scale estimation of additional reinforcement cost from three-phase imbalance considering thermal constraints[J]. *IEEE Trans Power Syst* 2016, 32(5): 3912-3923.
- [15] Pajic S, Emanuel A E. Effect of neutral path power losses on the apparent power definitions: A preliminary study[J]. *IEEE Trans Power Del* 2009, 24(2): 517-523.
- [16] Watson J D, Watson N R, Lestas I. Optimized dispatch of energy storage systems in unbalanced distribution networks[J]. *IEEE Trans Sustain Energy* 2017, 9(2): 639-650.
- [17] Fang L R, Ma K, Li R, Wang Z Y, Shi H. A statistical approach to estimate imbalance-induced energy losses for data-scarce low voltage networks[J]. *IEEE Trans Power Syst* 2019, 34(4): 2825-2835.
- [18] Data and code for three phase imbalance network. 2021. [Online]. Available: <https://github.com/wuhanichina/Imbalance-3-Phase>
- [19] Wu H, Yuan Y, Ma K, Fang L. Estimate the Probability Distribution of Imbalance-Induced Energy Loss With Minimal Data[J]. *IEEE Trans Power Syst* 2021, 36(4): 3798-3801.
- [20] Dahal S, Salehfar H. Impact of distributed generators in the power loss and voltage profile of three phase unbalanced distribution network[J]. *Int J Electr Power Energy Syst* 2016, 77: 256-262.
- [21] Wang M D, Zhang X, Zhao T, Zhuang F S, Wang F S, Qian N X, et al. Module power balance control strategy for three-phase cascaded H-bridge PV inverter under unbalanced grid voltage condition[J]. *IEEE Trans Emerg Sel Topics Power Electron* 2021, 9(5): 5657-5671.
- [22] Harley R G, Makram E B, Duran E G. The effects of unbalanced networks and unbalanced faults on induction motor transient stability[J]. *IEEE Trans Energy Convers* 1988, 3(2): 398-403.
- [23] Moradian M, Soltani J. An isolated three-phase induction generator system with dual stator winding sets under unbalanced load condition[J]. *IEEE Trans Energy Convers* 2016, 31(2): 531-539.
- [24] Li K, Liu J J, Wang Z A, Wei B. Strategies and operating point optimization of STATCOM control for voltage unbalance mitigation in three-phase three-wire systems[J]. *IEEE Trans Power Del* 2006, 22(1): 413-422.
- [25] Zhu J, Chow M Y, Zhang F. Phase balancing using mixed-integer programming [J]. *IEEE Trans Power Syst* 1998, 13(4): 1487-1492.
- [26] Zhu J X, Bilbro G, Chow M Y. Phase balancing using simulated annealing[J]. *IEEE Trans Power Syst* 1999, 14(4): 1508-1513.
- [27] Zeng X J, Zhai H F, Wang M X, Yang M, Wang M Q. A system optimization method for mitigating three-phase imbalance in distribution network[J]. *Int J Electr Power Energy Syst* 2019, 113: 618-633.
- [28] Yan S, Tan S C, Lee C K, Chaudhuri B, Hui S Y R. Electric springs for reducing power imbalance in three-phase power systems[J]. *IEEE Trans Power Electron* 2014, 30(7): 3601-3609.
- [29] Nour A M M, Helal A A, El-Saadawi M M, Hatata A Y. A control scheme for voltage unbalance mitigation in distribution network with rooftop PV systems based on distributed batteries[J]. *Int J Electr Power Energy Syst* 2021, 124: 106375.
- [30] Nejabatkhah F, Li Y W, Wu B. Control strategies of three-phase distributed generation inverters for grid unbalanced voltage compensation[J]. *IEEE Trans Power Electron* 2015, 31(7): 5228-5241.
- [31] Zheng Z Y, Guo M F, Yang N C, Jin T. Single-phase flexible arc suppression device based on BSC-SOGI-PLL method for distribution networks[J]. *Int J Electr Power Energy Syst* 2020, 121: 106100.
- [32] Fang Y, Fei J, Ma K. Model reference adaptive sliding mode control using RBF neural network for active power filter[J]. *Int J Electr Power Energy Syst* 2015, 73: 249-258.
- [33] Yu Y, Zhang C. Bifurcation analysis of cascaded H-bridge converter controlled by proportional resonant[J]. *Int J Electr Power Energy Syst* 2021, 125: 106476.